Assessment of the diagnostic performance of ^{18}F-FDG-PET/CT for detection and characterization of solid renal malignancies

Zein Nakhoda[1*] MD, MBA, Drew A. Torigian[1*] MD, MA, Babak Saboury[1] MD, MPH, Frank Hofheinz[2] PhD, Abass Alavi MD[1], MD(Hon.), PhD(Hon.), DSc (Hon.)

**Please note, the 1st 2 authors have contributed equally to the manuscript.*

1. Hospital of the University of Pennsylvania, Philadelphia, PA
2. PET Center, Institute of Radiopharmacy, Helmholtz-Zentrum Dresden-Rossendorf, Dresden, Germany

***

Keywords: Renal malignancy - Renal cell carcinoma (RCC) - Lymphoma - Metastases - ^{18}FDG-PET/CT

Correspondence address:
Drew A. Torigian MD MA
Department of Radiology
Hospital of the University of Pennsylvania, 3400 Spruce Street, Philadelphia, PA 19104
Tel: 215-615-3805
Fax: 215-614-0033
Email: Drew.Torigian@uphs.upenn.edu

Received:
5 October 2012
Accepted:
14 November 2012

Abstract

To evaluate the sensitivity of the positron emission tomography (PET) portion of fluorine-18 fluorodeoxyglucose-PET-computerized tomography (^{18}F-FDG-PET/CT) to detect solid malignant renal masses, and to assess for metabolic differences based on histopathological type. *Nineteen subjects* with 25 known solid malignant renal masses who underwent ^{18}F-FDG-PET/CT were retrospectively evaluated. Qualitative analysis of the PET portion only of ^{18}F-FDG-PET/CT examinations to assess visual detection of renal masses was initially performed in blinded fashion. Subsequently, measurements of standardized uptake value (SUV) and lesion-to-background ratios were performed for all masses and compared between histopathological types. Of 25 solid malignant renal masses, 18 were renal cell carcinoma (RCC), 3 were renal lymphoma, and 4 were metastases. *Twenty-two of 25 were detectable*, and all were correctly spatially localized. Fifteen of 22 detectable lesions were exophytic in configuration. The three non-detectable masses were non-exophytic RCC's with average diameter of 2.0cm. Fifteen of 18 of RCC were detectable, whereas all renal lymphomas and metastases were detectable. None of the metabolic parameters were statistically significant between RCC and renal lymphoma. However, all metabolic parameters were statistically significantly greater for renal metastases compared to RCC and renal lymphoma, and for clear cell RCC compared to papillary RCC. *In conclusion*, the PET portion of ^{18}F-FDG-PET/CT had a sensitivity of 88% for detection of solid malignant renal lesions in patients with known renal malignancy, and reveals differences in metabolic activity based on histopathological type, which may be useful for purposes of individualized medicine. Further studies are required for more in depth assessment of these preliminary observations.

Hell J Nucl Med 2013; 16(1): 19-24 *Epub ahead of print: 26-3-2013* *Published on line: 10 April 2013*

Introduction

Renal cancer accounts for about 2% of all cancers, with a steadily rising incidence from 7.1 per 100,000 in the early 1980s to 15.1 per 100,000 in 2009 [1-3]. The rise is partly due to the increased use of imaging procedures, such as ultrasonography (US), computed tomography (CT), and magnetic resonance imaging (MRI), resulting in incidental diagnosis of more malignant renal masses [4-6]. While the majority of malignant renal masses are due to renal cell carcinoma (RCC), metastases to the kidney and secondary renal involvement by lymphoma are not uncommon. For example, in one retrospective study of patients with renal masses diagnosed in the setting of a non-renal malignancy, 59% had a primary malignant renal tumor, 12% had a primary benign renal tumor, and 19% had metastases from the non-renal malignancy [7]. Overall, 7%-20% of patients with cancer are found to have renal metastases at autopsy, which most commonly originate from the lung, breast, stomach, pancreas, and colon, but which can also arise from the skin, liver, prostate, thyroid, and esophagus [8-16]. Similarly, secondary renal involvement by lymphoma, usually of non-Hodgkin's type, may be detected in 3%-8% of patients undergoing diagnostic CT [17].

Fluorine-18-2-fluoro-2-deoxy-D-glucose (^{18}F-FDG) positron emission tomography (PET) is a molecular imaging modality that is the current mainstay for the management of patients with various types of cancer [18]. However, it has been much less utilized for purposes of detecting and characterizing renal malignancies. In fact, there are only a handful of studies regarding the evaluation of renal malignancies using ^{18}F-FDG-PET, which have shown variability in diagnostic performance for the detection and characterization of renal cancer, and to date, there has been only one study of the diagnostic performance of ^{18}F-FDG-PET/CT for the evaluation of renal masses [19]. Therefore, the aim of the present study was to evaluate the sensitivity of the PET portion of PET/CT to detect solid renal malignancies in a cohort of subjects who had undergone both ^{18}F-FDG-PET/CT and diagnostic contrast-enhanced CT or magnetic resonance imaging (MRI), and to assess the potential

utility of ^{18}F-FDG-PET/CT to reveal differences in tumor metabolism between various histopathological types of renal malignancy.

Materials and methods

Subject population

This retrospective study was conducted following approval from the Institutional Review Board at the Hospital of the University of Pennsylvania along with a Health Insurance Portability and Accountability Act (HIPAA) waiver. A search of our radiology database from 2006 to 2012 was performed to identify subjects who previously underwent diagnostic quality contrast-enhanced abdominal CT or abdominal MRI with imaging findings characteristic of solid renal malignancy and who had also undergone ^{18}F-FDG-PET/CT for various other oncological indications. Subsequently, a search of our pathology database was performed to obtain histopathological confirmation of the diagnosis of solid renal malignancy when available.

A total of 19 subjects (13 men, 6 women, mean age 63.9, age range 47-87) with 25 solid malignant renal masses 18 due to RCC, 3 due to secondary involvement by lymphoma (marginal zone lymphoma in 1 and diffuse large B-cell lymphoma (DLBCL) in the other 2), and 4 due to metastases to the kidney (all from lung cancer)] were identified and assessed for the purpose of this study. Histopathological results were available for 14 of 25 lesions (12 RCC, 1 lymphoma, and 1 metastasis). The diagnoses for the other 11 lesions were established based on diagnostic CT and/or MRI and/or follow-up imaging features along with available clinical information. Fluorine-18-FDG-PET/CT and diagnostic abdominal CT or MRI studies were performed within a 4 month interval for all subjects except for 1 in whom there was a 3.5 year interval (although no change in the size of the renal lesion was seen between the CT portion of the PET/CT examination and the diagnostic abdominal CT study).

Fluorine-18-FDG-PET/CT image acquisition

A 16 detector-row LYSO whole-body PET/CT scanner with time-of-flight capabilities (Gemini TF, Philips Healthcare, Bothell, WA) was used to acquire ^{18}F-FDG-PET/CT images. ~555MBq of ^{18}F-FDG were administered intravenously for 3min per bed position. ~60min thereafter, 3D PET emission data were acquired from the skull base to mid thighs. A list-mode maximum-likelihood expectation-maximization (ML-EM) algorithm was utilized to perform image reconstruction. The system model included time-of-flight, normalization, randoms, attenuation, and scatter corrections. Attenuation correction of PET images was done utilizing rescaled low-dose CT. Images from PET and CT were reconstructed at 5mm slice thickness.

Fluorine-18-FDG-PET/CT image analysis

A board certified radiologist (DAT) with ~7 years of experience in the interpretation of PET/CT studies was blinded to the diagnostic abdominal CT and MRI results as well as to the low dose CT portion of the ^{18}F-FDG-PET/CT examinations, and performed qualitative assessments based on the PET portion only of the PET/CT examinations using a dedicated PET/CT analysis workstation (Extended Brilliance Workstation, Philips Healthcare, Bothell, WA). PET images were visually assessed for the presence and location (left vs. right; upper vs. mid pole vs. lower pole) of areas of focal ^{18}F-FDG uptake in the kidneys greater than background activity levels that appeared to be separate from the renal collecting systems. These results were then compared to the accompanying diagnostic abdominal CT or MRI studies and to the low dose CT portions of the PET/CT examinations to establish the accuracy of lesion localization. The sizes and configuration (exophytic vs. non-exophytic) of renal lesions were also then recorded based on measurements from CT or MRI.

Quantitative assessments based on the PET portion only of the PET/CT examinations were then performed. When feasible, 3D spherical masks were manually placed about each lesion in the kidney, while taking care to avoid the renal collecting system, in order to automatically delineate and quantify lesional regions of interest (ROI) using an automatic adaptive thresholding method via the software Region of interest visualization, evaluation, and image registration (ROVER) (ABX GmbH, Radeberg, Germany) [20-22]. This was possible for 22 out of 25 lesions that were visible on ^{18}F-FDG-PET/CT. The settings were restricted to those ROI with a minimum volume of 1cc and an initial threshold setting of 40% of maximum lesional metabolic activity. All other settings were left on default and "automatic" mode except for one lesion in which "threshold" mode was used, and the reconstructed image resolution was estimated at 8mm. Maximum standardized uptake value (SUVmax), mean standardized uptake value (SUVmean), and partial volume corrected mean standardized uptake value (corrected SUVmean) were automatically calculated by the software for each renal lesion.

Subsequently, in each patient, a 2.6cm in diameter 3D spherical mask was placed in the liver parenchyma to calculate background liver SUVmean, and a 1.4cm in diameter 3D spherical mask was placed in the renal parenchyma on the same side as each lesion while avoiding the collecting systems to calculate background renal parenchymal SUVmean. Lesion to background ratios were then calculated for all renal masses as lesion SUVmean/liver SUVmean (LBRliver) and lesion SUVmean/renal SUVmean (LBRkidney), respectively.

Statistical analysis

Tabulations of means and ranges of lesional maximal diameters, as well as averages, standard deviations, and ranges of SUVmax, SUVmean, partial volume corrected SUVmean, LBRliver, and LBRkidney were performed. Sensitivity of detection and accuracy of renal mass localization based on PET/CT analyses were also calculated. Comparisons for statistically significant differences between the average metabolic parameters for RCC, renal lymphoma, and renal metastasis were performed using unpaired t tests, and comparisons for statistically significant differences between metabolic parameters for the two encountered histopathological subtypes of RCC were also performed using unpaired t tests. A P value of < 0.05 was considered as statistically significant. All statistical analyses were performed using software (Microsoft Office Excel 2007, Microsoft, Redmond, WA).

Results

Twenty-two of 25 solid malignant renal masses (average maximal diameter 3.7cm±1.8cm, range 1.2-8.1cm) were visually detectable on the PET portion only of ^{18}F-FDG-PET/

CT (average SUVmax 9.7±8.6, range 1.8-29.9; average SUVmean 5.7±4.9, range 1.1-17.2; average partial volume corrected SUVmean 9.5±7.8, range 1.1-25.9; average LBRliver 2.9±2.6, range, 0.7-9.1; average LBRkidney 3.6±3.2, range 0.9-12.0), with 15 of 22 having an exophytic configuration in the kidney. Partial volume correction increased uncorrected SUVmean measurements for the renal lesions by an average of 78.2%±16.6%. All 22 masses were correctly localized based on visual assessment with respect to the side of renal involvement and spatial localization within the kidney. Eleven of 22 were found on the right, and 11 of 22 were found on the left. Nine of 22 were found in the upper pole, 6 of 22 in the mid pole, and 7 of 22 in the lower pole. Fifteen of 18 of RCC were visually detectable (Fig. 1), whereas 3 of 3 of renal lymphomas (Fig. 2) and 4 of 4 of renal metastases (Fig. 3) were visually detectable. The three remaining masses (average diameter 2.0±0.25cm, range 1.7-2.2cm) that were not visually detectable on the PET portion only of ^{18}F-FDG-PET/CT were all non-exophytic in configuration, located in the right mid pole, right lower pole, and left mid pole, and all were due to RCC (two papillary subtype and one of unknown subtype). These three lesions could not be delineated with software, and therefore SUV measurements for these lesions could not be calculated semi-automatically. No false positive detections of renal lesions based on PET only images from ^{18}F-FDG-PET/CT were reported based on visual assessment.

Average maximal diameter, SUVmax, SUVmean, and partial volume corrected SUVmean were 3.6±2.1cm, 7.4±7.1, 4.4±4.0, and 8.5±7.6, respectively, for renal RCC; 3.6±1.0cm, 6.3±3.3, 3.5±1.5, and 5.1±2.9, respectively, for renal lymphoma; and 4.2±1.2cm, 21.1±7.8, 11.8±5.1, and 16.8±7.4, respectively, for renal metastases. None of the metabolic parameters were statistically significant between RCC and renal lymphoma. However, all of the metabolic parameters were statistically significant between RCC and renal metastases (P=0.002, 0.002, 0.034, 0.003, and 0.014 for SUVmax, SUVmean, partial volume corrected SUVmean, LBRliver, and LBRkidney, respectively) and between renal lymphoma and renal metastases (P=0.022, 0.029, 0.043, 0.033, 0.028 for SUVmax, SUVmean, partial volume corrected SUVmean, LBRliver, and LBRkidney, respectively).

Among the 8 RCC lesions with available histopathological subtype results, average diameter, SUVmax, SUVmean, and partial volume corrected SUVmean were 3.6±2.5cm, 4.4±3.0, 2.9±1.7, and 5.4±3.4 for those of papillary subtype (6 lesions), respectively, and 5.1±4.2cm, 16.0±15.6, 8.6±8.2, and 16.0±13.2 for those of clear cell subtype (2 lesions), respectively. All metabolic parameters were statistically significantly different between papillary and clear cell subtypes of RCC (P=0.003, 0.004, 0.004, 0.001, and 0.001 for SUVmax, SUVmean, partial volume corrected SUVmean, LBRliver, and LBRkidney, respectively).

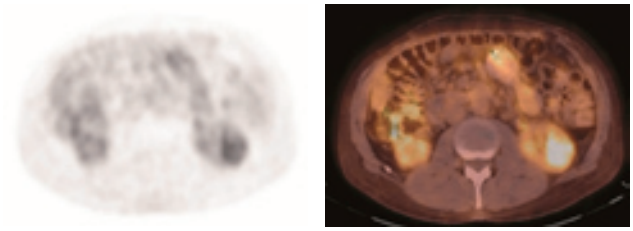

Figure 1. A 48 year old man with papillary RCC. Axial ^{18}F-FDG-PET and fused PET/CT images reveal 3.8cm mildly ^{18}F-FDG avid mass in interpolar left kidney with SUVmax 3.7, SUVmean 2.9, partial volume corrected SUVmean 7.9, LBRliver 1.8, and LBRkidney 2.1.

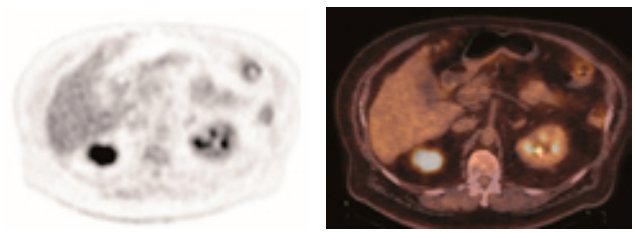

Figure 2. A 68 year old man with DLBCL and secondary involvement of kidney by lymphoma. Axial ^{18}F-FDG-PET (A) and fused PET/CT (B) images show 4.1cm ^{18}F-FDG avid mass in upper pole of right kidney with SUVmax 7.7, SUVmean 4.7, partial volume corrected SUVmean of 7.5, LBRliver 2.2, and LBRkidney 2.6.

Discussion

The classic clinical triad of flank pain, a palpable mass, and hematuria in association with renal cancer is relatively uncommon (occurring in only 5%-10% of patients), as the vast majority of renal masses are now detected incidentally through widespread use of cross-sectional structural imaging techniques including CT, MRI, and US [23]. CT is typically used as the primary imaging modality for characterization of an indeterminate renal mass, although MRI and US are alternative imaging modalities that are also useful, particularly in patients who have contraindications to contrast-enhanced CT (such as in those with an allergy to iodinated contrast medium) and for the evaluation of pediatric and pregnant patients given the lack of radiation dose [23].

FDG-PET is a molecular imaging modality that is useful for the management of patients with various types of cancer, and provides information that is complementary with that provided by structural imaging techniques [18]. Wahl et al first demonstrated the feasibility of ^{18}F-FDG-PET for imaging

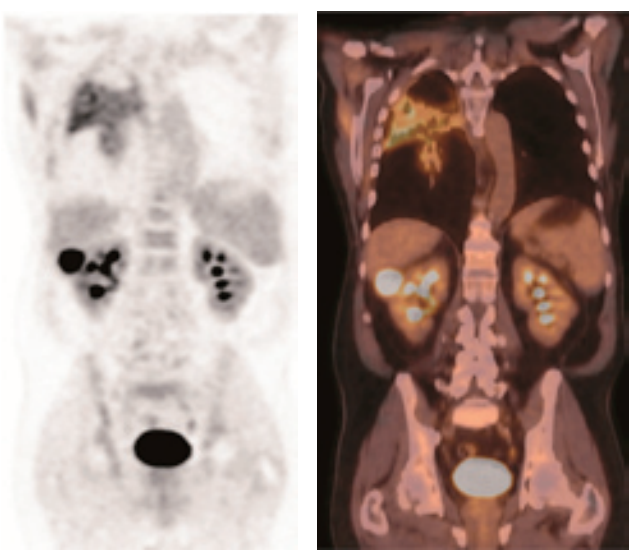

Figure 3. A 70 year old man with lung cancer metastatic to right kidney. Coronal ^{18}F-FDG-PET and fused PET/CT images demonstrate exophytic 3.0cm^{18}F-FDG avid mass in interpolar right kidney with SUVmax 20.5, SUVmean 10.7, partial volume corrected SUVmean of 13.9, LBRliver 5.4, and LBRkidney 6.3. Mildly ^{18}F-FDG avid radiation change is also seen in right upper lobe of lung.

primary and metastatic renal cancer in a murine xenograft model as well as in 5 patients [24]. However, the reported sensitivities and specificities of ^{18}F-FDG-PET in subsequent studies have generally been suboptimal in comparison to diagnostic CT or MRI, with sensitivities ranging from 40%-94% and specificities ranging from 0%-100% [25-35]. The low sensitivity of ^{18}F-FDG-PET in some reports has been attributed to FDG excretion through the kidneys and collecting systems, decreasing contrast between renal lesions and normal tissues, as well as due to significant variability of ^{18}F-FDG uptake that may be related to variable expression of GLUT-1 glucose transporters, tumor grade, presence of central necrosis, and/or lack of accessibility of ^{18}F-FDG [26, 28, 30, 33, 36].

There is only one prior report in the literature that reports the diagnostic performance of ^{18}F-FDG-PET/CT for evaluation of malignant renal masses. Other researchers prospectively studied 18 patients with suspicious primary renal masses detected on CT, MRI, or US by using ^{18}F-FDG-PET/CT. Of the 15 patients with who had RCC, 14 were of clear cell subtype and 1 was of papillary subtype. Fluorine-18-FDG-PET/CT had a sensitivity, specificity, and accuracy of 46.6%, 66.6%, and 50%, respectively [19]. In our study, however, we demonstrated an overall sensitivity of 88% for detection of solid renal malignancies with sensitivities of 83%, 100%, and 100% for RCC, secondary renal lymphomas, and renal metastases, respectively. As we did not include subjects with non-malignant renal masses in this study, we were not able to calculate the specificity of ^{18}F-FDG-PET/CT. These favorable diagnostic results, despite the renal excretion of ^{18}F-FDG, may in part be related to the time-of-flight technology that is available on the PET/CT scanner that was utilized and due to selection of subjects with known solid renal malignancies. However, given these preliminary results, further evaluation of the diagnostic performance of ^{18}F-FDG-PET/CT for detection of renal masses is warranted.

Several reports in the literature have previously assessed for differences in the metabolic properties of various histopathological types of renal malignancy using either ^{18}F-FDG-PET or ^{18}F-FDG-PET/CT. Other researchers studied 13 patients with suspicious renal masses using ^{18}F-FDG and a dual head coincidence mode gamma camera, and reported an LBRkidney range of 1.0-1.8 for RCC compared to 3.0-4.4 for renal carcinosarcoma [33]. Other researchers studied 10 patients with solid renal malignancies using ^{18}F-FDG-PET and reported that the average LBRkidney for renal lymphoma was 4.5 compared to 2.2 for RCC [32]. Ye et al studied 12 patients with renal lymphoma (7 DLBCL, 2 B-cell lymphoma, 1 T-cell lymphoma, 2 T/NK-cell lymphoma) and 12 patients with RCC (5 clear cell subtype, 7 other subtypes) using ^{18}F-FDG-PET/CT. They reported that ^{18}F-FDG uptake was much greater in renal lymphoma compared to clear cell RCC (average SUVmean 6.37±2.28 vs. 2.58±0.62, respectively), although no gross difference in ^{18}F-FDG uptake between renal lymphoma and RCC of all subtypes (average SUVmean 6.37±2.28 vs. 6.27±1.15, respectively) was noted [37]. Kumar et al studied 28 solid renal masses [10 primary renal malignancies and 18 secondary renal malignancies (11 lymphoma, 7 metastases)] in 24 patients using ^{18}F-FDG-PET, and reported no statistically significant difference between the average SUVmax and SUVmean for primary renal malignancies (7.9±4.9 and 6.0±3.6, respectively), and those for secondary renal malignancies (6.1±3.4 and 4.7±2.8, respectively) [35]. In our study, we observed that RCC and secondary renal lymphoma had similar metabolic activities, whereas renal metastases had significantly greater levels of metabolism compared to RCC and secondary renal lymphoma.

Several reports in the literature have also previously assessed for differences in the metabolic properties of various subtypes of RCC using either ^{18}F-FDG-PET or ^{18}F-FDG-PET/CT. Researchers reported that the Fuhrman grade of ^{18}F-FDG-positive malignant renal lesions based on PET/CT was statistically significantly higher compared to that of ^{18}F-FDG-negative lesions [19]. Other researchers studied 26 patients with RCC (19 of clear cell subtype and 7 of non-clear cell subtype) using ^{18}F-FDG-PET/CT, and reported an average SUVmax of 3.9 (range 1.7-9.5) for clear cell RCC and 7.9 (range 2.7-13.9) for non-clear cell RCC, which was borderline significantly different (P=0.08) [38]. Other researchers studied 11 patients with RCC using ^{18}F-FDG-PET, and reported that patients with positive ^{18}F-FDG uptake at the primary tumor site had higher tumor grades (P=0.018) and a tendency towards higher GLUT-1 expression (P=0.071) than patients with negative PET results [36]. However, other researchers studied 19 patients with RCC using ^{18}F-FDG-PET, and reported that there is no correlation between GLUT-1 expression and ^{18}F-FDG-PET positivity [30]. Similarly, other researchers studied 35 patients with ^{18}F-FDG-PET for characterization and staging of a suspicious renal mass, and reported that the distribution of Fuhrman histological grades among visualized and non-visualized RCC on ^{18}F-FDG-PET was not statistically significant [28]. In our study, we observed that the clear cell RCC subtype had significantly greater levels of metabolism compared to those of the papillary RCC subtype. This suggests that ^{18}F-FDG-PET/CT may be useful to assess RCC tumor biology, which may have implications for patient management. For example, other researchers reported that clear cell RCC with lower baseline SUVmax are more likely to respond to neoadjuvant therapy with sorafenib, whereas this trend was not observed for non-clear cell RCC subtypes [38].

To our knowledge, our study is the first in the literature to assess the effects of partial volume correction upon SUV measurements of renal lesions, as well as the differences in partial volume corrected SUV between different histopathological types of renal malignancy, through use of semi-automated software. Partial volume correction is important since measurement of lesional SUV is susceptible to the partial volume effect due to image blurring and image sampling. As such, this effect generally leads to underestimation of lesional metabolic activity and overestimation of lesional size, especially for small lesions with size $\leq$2-3 times full-width-at-half-maximum (FWHM) of the reconstructed image resolution [39-43]. Unfortunately, partial volume correction of SUV measurements is currently not performed in routine clinical practice, potentially leading to significant errors in disease quantification. In the current study, we demonstrated that partial volume correction of SUVmean led to an average increase of 78.2% in the SUVmean of solid renal malignancies.

This study has several limitations. First, the study was performed retrospectively utilizing a small cross-sectional sample of subjects with known renal malignancies, potentially leading to selection and other unknown biases. As such, the diagnostic performance results of ^{18}F-FDG-PET/CT reported in this study is not necessarily generalizable to the general

population with indeterminate renal lesions, but instead applies to those patients with a known renal malignancy. Second, histopathological verification of renal malignancy was only available in 56% of lesions, such that the diagnosis of renal malignancy was assumed in the other 44% of lesions based on diagnostic CT and/or MRI and/or follow-up imaging features along with available clinical information. However, diagnostic CT and MRI have been shown to have high accuracy for characterization of renal lesions as malignant, and therefore we believe that the error from this potential verification bias is minimal.

In conclusion, the PET portion of ^{18}F-FDG-PET/CT had a sensitivity of 88% for the detection of solid malignant renal lesions in patients with known renal malignancy, despite the renal excretion of ^{18}F-FDG. In addition, ^{18}F-FDG-PET/CT demonstrated some differences in metabolic activity based on renal tumor histopathological type and RCC subtype, which may be useful for purposes of individualized medicine. Furthermore, measurement of partial volume corrected SUVmean of renal malignancies is feasible from the PET portion of ^{18}F-FDG-PET/CT scans through use of semi-automated image analysis software. Further larger scale studies are required for more in depth assessment of these preliminary observations.

The authors declare that they have no conflicts of interest.

Bibliography

1. Ferlay J, Shin HR, Bray F et al. Estimates of worldwide burden of cancer in 2008: GLOBOCAN 2008. *Int J Cancer* 2010; 127: 2893-917. doi:10.1002/ijc.25516.
2. Hollingsworth JM, Miller DC, Daignault S, Hollenbeck BK. Rising incidence of small renal masses: a need to reassess treatment effect. *J Natl Cancer Inst* 2006 ; 98: 1331-4. doi:10.1093/jnci/djj362.
3. Howlader N NA, Krapcho M, Neyman N et al. *SEER Cancer Statistics Review, 1975-2009* (Vintage 2009 Populations), National Cancer Institute, Bethesda, MD, http://seer.cancer.gov/csr/1975_2009_pops09/, based on November 2011 SEER data submission, posted to the SEER web site, April 2012. 2011.
4. Jayson M, Sanders H. Increased incidence of serendipitously discovered renal cell carcinoma. *Urology* 1998; 51: 203-5.
5. Bretheau D, Lechevallier E, Eghazarian C et al. Prognostic significance of incidental renal cell carcinoma. *Eur Urol* 1995; 27: 319-23.
6. Homma Y, Kawabe K, Kitamura T et al. Increased incidental detection and reduced mortality in renal cancer--recent retrospective analysis at eight institutions. *Int J Urol* 1995; 2: 77-80.
7. Sanchez-Ortiz RF, Madsen LT, Bermejo CE et al. A renal mass in the setting of a nonrenal malignancy: When is a renal tumor biopsy appropriate? *Cancer* 2004; 101: 2195-201. doi:10.1002/cncr.20638.
8. Takehara K, Koga S, Nishikido M et al. Breast cancer metastatic to the kidney. *Anticancer Res* 1999; 19: 5571-3.
9. Pollack HM, Banner MP, Amendola MA. Other malignant neoplasms of the renal parenchyma. *Semin Roentgenol* 1987; 22: 260-74.
10. Aron M, Nair M, Hemal AK. Renal metastasis from primary hepatocellular carcinoma. A case report and review of the literature. *Urol Int* 2004; 73: 89-91. doi:10.1159/000078812.
11. Trompette A, Clavel M, Paraf F et al. Symptomatic renal metastases of bronchial carcinoma. *Rev Mal Respir* 1999; 16: 833-5.
12. Denti F, Wisard M, Guillou L et al. Renal metastasis from prostatic adenocarcinoma: a potential diagnostic pitfall. *Urol Int* 1999; 62: 171-3.
13. Martino L, Martino F, Coluccio A et al. Renal metastasis from pancreatic adenocarcinoma. *Arch Ital Urol Androl* 2004; 76: 37-9.
14. Muller HJ, Weckesser M, Schober O. Bilateral renal metastasis in follicular thyroid carcinoma. *Nuklearmedizin* 2000; 39: 45-7.
15. Ho L, Wassef H, Henderson R, Seto J. Renal metastasis from primary colon cancer on FDG PET-CT. *Clin Nucl Med* 2009; 34: 596-7. doi:10.1097/RLU.0b013e3181b06cb3.
16. Bracken RB, Chica G, Johnson DE, Luna M. Secondary renal neoplasms: an autopsy study. *South Med J* 1979; 72: 806-7.
17. Urban BA, Fishman EK. Renal lymphoma: CT patterns with emphasis on helical CT. *Radiographics* 2000; 20: 197-212.
18. Kwee TC, Basu S, Saboury B et al. Functional oncoimaging techniques with potential clinical applications. *Front Biosci (Elite Ed)* 2012; 4: 1081-96. doi:443 [pii].
19. Ozulker T, Ozulker F, Ozbek E, Ozpacaci T. A prospective diagnostic accuracy study of F-18 fluorodeoxyglucose-positron emission tomography/computed tomography in the evaluation of indeterminate renal masses. *Nucl Med Commun* 2011; 32: 265-72. doi:10.1097/MNM.0b013e3283442e3b.
20. Torigian DA, Lopez RF, Alapati S et al. Feasibility and performance of novel software to quantify metabolically active volumes and 3D partial volume corrected SUV and metabolic volumetric products of spinal bone marrow metastases on ^{18}F-FDG-PET/CT. *Hell J Nucl Med* 2011; 14: 8-14.
21. Hofheinz F, Potzsch C, Oehme L et al. Automatic volume delineation in oncological PET. Evaluation of a dedicated software tool and comparison with manual delineation in clinical data sets. *Nuklearmedizin* 2012; 51: 9-16. doi:10.3413/Nukmed-0419-11-07.
22. Hofheinz F, Langner J, Petr J et al. A method for model-free partial volume correction in oncological PET. *EJNMMI research* 2012; 2: 16. doi:10.1186/2191-219X-2-16.
23. Ng CS, Wood CG, Silverman PM et al. Renal cell carcinoma: diagnosis, staging, and surveillance. *Am J Roentgenol* 2008; 191: 1220-32. doi:10.2214/AJR.07.3568.
24. Wahl RL, Harney J, Hutchins G, Grossman HB. Imaging of renal cancer using positron emission tomography with 2-deoxy-2-^{18}F-fluoro-D-glucose: pilot animal and human studies. *J Urol* 1991; 146: 1470-4.
25. Martinez de Llano SR, Delgado-Bolton RC, Jimenez-Vicioso A et al. Meta-analysis of the diagnostic performance of ^{18}F-FDG PET in renal cell carcinoma. *Rev Esp Med Nucl* 2007; 26: 19-29.
26. Bachor R, Kotzerke J, Gottfried HW et al. Positron emission tomography in diagnosis of renal cell carcinoma. *Urologe A* 1996; 35: 146-50.
27. Kocher F, Hauptmann R, Reske S. Preoperative lymph node staging in patients with kidney and urinary bladder neoplasm. *J Nucl Med* 1994; 35: 223P-4P.
28. Aide N, Cappele O, Bottet P et al. Efficiency of [^{18}F]FDG PET in characterising renal cancer and detecting distant metastases: a comparison with CT. *Eur J Nucl Med Mol Imaging* 2003; 30: 1236-45. doi:10.1007/s00259-003-1211-4.
29. Kang DE, White RL, Jr., Zuger JH et al. Clinical use of fluorodeoxyglucose F-18 positron emission tomography for detection of renal cell carcinoma. *J Urol* 2004; 171: 1806-9. doi:10.1097/01.ju.0000120241.50061.e4.
30. Miyakita H, Tokunaga M, Onda H et al. Significance of ^{18}F-fluorodeoxyglucose positron emission tomography (FDG-PET) for detection of renal cell carcinoma and immunohistochemical glucose transporter 1 (GLUT-1) expression in the cancer. *Int J Urol* 2002; 9: 15-8.

31. Ramdave S, Thomas GW, Berlangieri SU et al. Clinical role of F-18 fluorodeoxyglucose positron emission tomography for detection and management of renal cell carcinoma. *J Urol* 2001; 166: 825-30.
32. Goldberg MA, Mayo-Smith WW, Papanicolaou N et al. FDG PET characterization of renal masses: preliminary experience. *Clin Radiol* 1997; 52: 510-5.
33. Montravers F, Grahek D, Kerrou K et al. Evaluation of FDG uptake by renal malignancies (primary tumor or metastases) using a coincidence detection gamma camera. *J Nucl Med* 2000; 41: 78-84.
34. Ak I, Can C. F-18 FDG PET in detecting renal cell carcinoma. *Acta Radiol* 2005; 46: 895-9.
35. Kumar R, Chauhan A, Lakhani P et al. 2-Deoxy-2-[F-18]fluoro-D-glucose-positron emission tomography in characterization of solid renal masses. *Mol Imaging Biol* 2005; 7: 431-9.
36. Miyauchi T, Brown RS, Grossman HB et al. Correlation between visualization of primary renal cancer by FDG-PET and histopathological findings. *J Nucl Med* 1996; 37: 64P.
37. Ye XH, Chen LH, Wu HB et al. ^{18}F-FDG PET/CT evaluation of lymphoma with renal involvement: comparison with renal carcinoma. *South Med J* 2010; 103: 642-9. doi:10.1097/SMJ.0b013e3181e23cb0.
38. Khandani AH, Cowey LC, Moore DT et al. Primary renal cell carcinoma: relationship between ^{18}F-FDG uptake and response to neoadjuvant sorafenib. *Nucl Med Commun* 2012. doi:10.1097/MNM.0b013e3283561837.
39. Hoffman EJ, Huang SC, Phelps ME. Quantitation in positron emission computed tomography: 1. Effect of object size. *J Comput Assist Tomogr* 1979; 3: 299-308.
40. Soret M, Bacharach SL, Buvat I. Partial-volume effect in PET tumor imaging. *J Nucl Med* 2007; 48: 932-45.
41. Basu S, Zaidi H, Houseni M et al. Novel quantitative techniques for assessing regional and global function and structure based on modern imaging modalities: Implications for normal variation, aging and diseased states. *Sem Nucl Med* 2007; 37: 223-39.
42. Hickeson M, Yun M, Matthies A et al. Use of a corrected standardized uptake value based on the lesion size on CT permits accurate characterization of lung nodules on FDG-PET. *Eur J Nucl Med Mol Imaging* 2002; 29: 1639-47.
43. Torigian DA, Chong E, Schuster S et al. Feasibility and utility of ROVER software for 3D quantitative image analysis of FDG-PET in patients with diffuse large B-cell lymphoma (DLBCL). *J Nucl Med* 2009; 50: 36P.